Particle Filter for Combined Wheel-Slip and Vehicle-Motion Estimation

Berntorp, Karl

Published in:
2015 American Control Conference (ACC)

DOI:
10.1109/ACC.2015.7172186

2015

Particle Filter for Combined Wheel-Slip and Vehicle-Motion Estimation

Karl Berntorp

***Abstract*— The vehicle-estimation problem is approached by fusing measurements from wheel encoders, an inertial measurement unit, and (optionally) a global positioning system in a Rao-Blackwellized particle filter. In total 14 states are estimated, including key variables in active safety systems, such as longitudinal velocity, roll angle, and wheel slip for all four wheels. The method only relies on kinematic relationships. We present experimental data for one test scenario, using a Volkswagen Golf equipped with state-of-the-art sensors for determining ground truth. We report highly promising results, even for periods of combined aggressive cornering and braking.**

I. Introduction

Automotive control systems have traditionally relied on their own set of sensors to estimate the states needed for the specific control application. With the improved computing and networking capabilities in modern vehicles during the last decade, the different systems are now able to exchange sensor information. Hence, sophisticated sensor-fusion techniques are now feasible alternatives in automotive systems.

This paper proposes a novel approach to model-based, joint wheel-slip and motion estimation of four-wheeled ground vehicles. The method fuses wheel-encoder, acceleration, gyro, and (optionally) global positioning system (GPS) position measurements to create estimates of the vehicle's pose, translational velocities, and wheel slip. We explicitly model the nonlinear slip dynamics in the state and measurement equations, and estimate the states with a marginalized particle filter [1]. The rationale is that by introducing a model of the slip propagation, better overall estimation performance can be obtained. The method only relies on kinematic relations, which implies that neither parameters describing the ground-wheel interaction, which otherwise need to be estimated for multiple terrain types [2], nor masses or inertias are required. One reason for introducing a particle filter is that the slip dynamics are highly nonlinearly dependent on the velocity. A particle filter is therefore suitable for this problem. Fig. 1 illustrates the typical relation between wheel slip and tire force.

Slip-estimation techniques are typically either rule based [3]; restricted to two-wheel drive [4], [5]; or assume knowledge of, or the need to estimate, physical vehicle parameters before being possible to use [3]. Linearizations of the force-slip curve was used in [6] to estimate the longitudinal tire stiffness. Motor-current based wheel slip detection was proposed in [7]. Moreover, [8] used a nine degrees-of-freedom vehicle model in a Kalman filter to estimate vehicle speed, brake forces, wheel slip, and vehicle sideslip angle. In [9], a roll-angle and road-bank estimation procedure using a proportional-integral observer was introduced, and in [10] an experimentally verified roll-angle estimation with accompanying stability proofs was presented. Roll-angle estimation was also considered in [11].

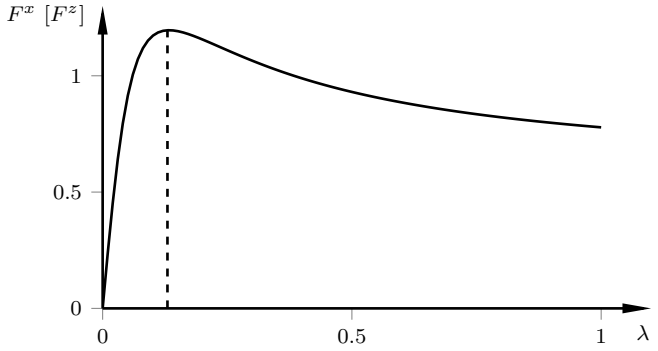

Fig. 1. Longitudinal force F^x as function of longitudinal wheel slip λ. ABS aim to control the wheel slip around, possibly time varying, reference values, determined by a high-level safety system. The behavior is stable to the left of the peak and unstable to the right of the peak. Hence, reliable estimates of the wheel slip is necessary for good performance.

II. Assumptions and Notation

Fig. 2 contains the schematics for a four-wheeled ground vehicle. Lower-case boldface letters indicate column matrices (or vectors). We assume planar motion (i.e., small inclination and road-bank angles). The composite rotation between the inertial frame $\mathcal{I}$ and the body-fixed frame $\mathcal{B}$ is described by a rotation ψ about $Z_{\mathcal{I}}$, followed by a rotation ϕ about the resulting $X_{\mathcal{V}}$-axis. A rotation matrix from $\mathcal{V}$ to $\mathcal{I}$ is denoted with $\boldsymbol{R}_{\mathcal{V}}^{\mathcal{I}}$. The superscript $\mathcal{V}$ as in $\boldsymbol{v}^{\mathcal{V}}$ means $\boldsymbol{v}$ with respect to $\mathcal{I}$, expressed in frame $\mathcal{V}$. Measurements of the longitudinal and lateral accelerations $\mathbf{a} \in \mathbb{R}^2$, wheel-angular velocities $\boldsymbol{\omega} \in \mathbb{R}^4$, steering-wheel angle, and roll and yaw rates $\boldsymbol{\xi} \in \mathbb{R}^2$ are available. These measurements can be considered standard for vehicles equipped with ABS, ESC, and a rollover-avoidance system. We do not assume, but can incorporate, GPS measurements in the presented framework. In this paper, δ_1 and δ_2 are found through the steering-wheel angle assuming a fixed gear ratio.

Karl Berntorp was with the Department of Automatic Control, Lund University, Lund, Sweden, at the time of this research. He is now with Mitsubishi Electric Research Laboratories, 02139 Cambridge, MA, USA. E-mail: karl.o.berntorp@ieee.org.

This work was not supported by Mitsubishi Electric or any of its subsidiaries. It was supported by the Swedish Foundation for Strategic Research through the project ENGROSS, the LCCC Linnaeus Center, and the ELLIIT Excellence Center at Lund University.

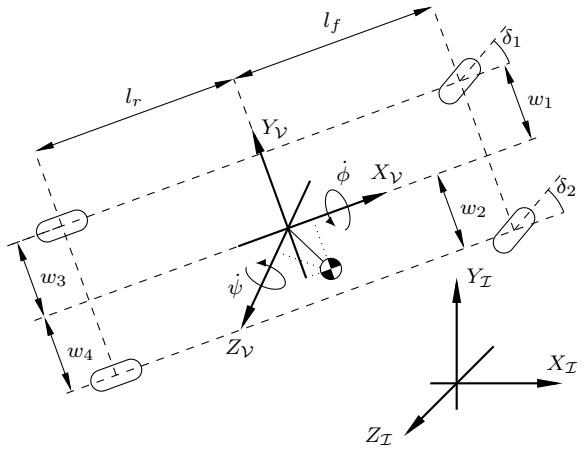

Fig. 2. The vehicle model and its degrees of freedom. The wheels are numbered from the front left wheel to the rear right wheel. The coordinate axes of the frames are denoted with capital letters.

III. Background on Particle Filters

Particle filters are sequential Monte-Carlo methods that represent the posterior probability density function $p(\boldsymbol{x}_{0:k}|\boldsymbol{y}_{0:k})$ of the state trajectory $\boldsymbol{x}_{0:k} := \{\boldsymbol{x}_0, \dots, \boldsymbol{x}_k\}$ given the measurements $\boldsymbol{y}_{0:k} := \{\boldsymbol{y}_0, \dots, \boldsymbol{y}_k\}$ with a set of weighted particles [12], [13]. This results in

$$p(\boldsymbol{x}_{0:k}|\boldsymbol{y}_{0:k}) \approx \sum_{i=1}^{N} w_k^i \delta(\boldsymbol{x}_{0:k} - \boldsymbol{x}_{0:k}^i).$$

Here, $\delta(\cdot)$ is the Dirac delta function and w_k^i is the associated weight for the ith particle given the measurements $\boldsymbol{y}_{0:k}$. The idea of the Rao-Blackwellized particle filter [1] is to estimate a subset of the states, $\boldsymbol{z}_k$, with a constrained Kalman filter, and apply the particle filter to the rest of the states. This is done by using the factorization

$$p(\boldsymbol{z}_k, \boldsymbol{\eta}_{0:k}|\boldsymbol{y}_{0:k}) = p(\boldsymbol{z}_k|\boldsymbol{\eta}_{0:k}, \boldsymbol{y}_{0:k}) p(\boldsymbol{\eta}_{0:k}|\boldsymbol{y}_{0:k}),$$

where $\boldsymbol{z}_k \in \mathbb{R}^{n_z}$ and $\boldsymbol{\eta}_k \in \mathbb{R}^{n_\eta}$ have the dynamics

$$\boldsymbol{z}_{k+1} = \boldsymbol{f}(\boldsymbol{\eta}_k) + \boldsymbol{A}(\boldsymbol{\eta}_k)\boldsymbol{z}_k + \boldsymbol{F}(\boldsymbol{\eta}_k)\boldsymbol{w}_k^{\boldsymbol{z}}, \tag{1a}$$
$$\boldsymbol{\eta}_{k+1} = \boldsymbol{g}(\boldsymbol{\eta}_k) + \boldsymbol{B}(\boldsymbol{\eta}_k)\boldsymbol{z}_k + \boldsymbol{G}(\boldsymbol{\eta}_k)\boldsymbol{w}_k^{\boldsymbol{\eta}}, \tag{1b}$$
$$\boldsymbol{y}_k = \boldsymbol{h}(\boldsymbol{\eta}_k) + \boldsymbol{C}(\boldsymbol{\eta}_k)\boldsymbol{z}_k + \boldsymbol{e}_k. \tag{1c}$$

The process noise $\boldsymbol{w}_k = \begin{bmatrix}(\boldsymbol{w}_k^{\boldsymbol{z}})^{\mathrm{T}} & (\boldsymbol{w}_k^{\boldsymbol{\eta}})^{\mathrm{T}}\end{bmatrix}^{\mathrm{T}}$ and the measurement noise $\boldsymbol{e}_k$ are assumed white and Gaussian distributed. Note that $\boldsymbol{z}_k$ is linear given $\boldsymbol{\eta}_{0:k}$. Inputs are introduced by modifying the mean of the process noise. The weighted mean of the particles is used to get a state estimate.

IV. Modeling

The mass center is assumed to be located at center of geometry (CoG). We do not make any assumptions on whether the vehicle is all-wheel drive.

Let the velocity of CoG with respect to frame $\mathcal{I}$ expressed in frame $\mathcal{V}$ be $\boldsymbol{v}^{\mathcal{V}} = \begin{bmatrix}v^{\mathcal{V},X} & v^{\mathcal{V},Y}\end{bmatrix}^{\mathrm{T}}$. The longitudinal velocity at the wheel-center contact point of wheel i is denoted with v_i^x and can be found through the kinematics. There exist several definitions for wheel slip. The longitudinal wheel slip for wheel i is here defined as

$$\lambda_i := 1 - \frac{R_i \omega_i}{v_i^x}, \quad \forall i \in \{1, \dots, 4\}, \tag{2}$$

where R_i is the wheel radius for wheel i. This definition implies that $\lambda_i \in (-\infty, 1]$.

A. Continuous-Time Dynamic Model

The minimum set of states to jointly estimate vehicle motion and wheel slip are the position $\boldsymbol{p} \in \mathbb{R}^2$, rotation $\boldsymbol{\psi} \in \mathbb{R}^2$, velocity $\boldsymbol{v} \in \mathbb{R}^2$, and the wheel slip $\boldsymbol{\lambda} \in \mathbb{R}^4$. The acceleration and gyro measurements $\boldsymbol{u_a}$ and $\boldsymbol{u_\xi}$ are used as inputs. Low-cost inertial measurement units (IMUs) suffer from biased measurements. Accelerometer and gyroscope bias are denoted with $\boldsymbol{b_a} = \begin{bmatrix}b_{\boldsymbol{a}}^X & b_{\boldsymbol{a}}^Y\end{bmatrix}^{\mathrm{T}}$ and $\boldsymbol{b_\xi} = \begin{bmatrix}b_{\boldsymbol{\xi}}^X & b_{\boldsymbol{\xi}}^Z\end{bmatrix}^{\mathrm{T}}$, respectively. For experiments lasting a couple of minutes, it is appropriate to model the bias as a random walk:

$$\dot{b} = w_b,$$

where the bias noise term w_b is white Gaussian with zero mean. The IMU measurements are therefore modeled as

$$\boldsymbol{u_a} = \boldsymbol{a}^{\mathcal{B}} + \boldsymbol{b_a} + \boldsymbol{g} + \boldsymbol{w_a}, \tag{3a}$$
$$\boldsymbol{u_\xi} = \boldsymbol{\xi}^{\mathcal{B}} + \boldsymbol{b_\xi} + \boldsymbol{w_\xi}, \tag{3b}$$

where $\boldsymbol{g} = \begin{bmatrix}0 & g\phi\end{bmatrix}^{\mathrm{T}}$ is the component vector from gravity caused by the roll angle ϕ. Moreover, $\boldsymbol{w_a}$ and $\boldsymbol{w_\xi}$ are modeled as zero-mean, white Gaussian noise. The kinematic equations for the position, velocity, and bias states are

$$\dot{\boldsymbol{p}} = \boldsymbol{v}, \tag{4a}$$
$$\dot{\boldsymbol{v}} = \boldsymbol{R}_{\mathcal{B}}^{\mathcal{I}}(\boldsymbol{u_a} - \boldsymbol{b_a} - \boldsymbol{g} + \boldsymbol{w_a}), \tag{4b}$$
$$\dot{\boldsymbol{b}}_{\boldsymbol{a}} = \boldsymbol{w}_{\boldsymbol{b_a}}, \tag{4c}$$
$$\dot{\boldsymbol{b}}_{\boldsymbol{\xi}} = \boldsymbol{w}_{\boldsymbol{b_\xi}}, \tag{4d}$$
$$\dot{\phi} = (u_{\boldsymbol{\xi}}^X - b_{\boldsymbol{\xi}}^X + w_{\boldsymbol{\xi}}^X), \tag{4e}$$
$$\dot{\psi} = u_{\boldsymbol{\xi}}^Z - b_{\boldsymbol{\xi}}^Z + w_{\boldsymbol{\xi}}^Z. \tag{4f}$$

The kinematic equations (4a)–(4d) describe the relation between the position $\boldsymbol{p}$ and velocity $\boldsymbol{v}$ expressed in the inertial frame $\mathcal{I}$ and the acceleration $\boldsymbol{a}^{\mathcal{B}}$ and associated bias $\boldsymbol{b_a}$ expressed in the body frame $\mathcal{B}$. The kinematic equations (4e)–(4f) describe the relation between the rotation angles with respect to $\mathcal{I}$ and the rotation rates $\boldsymbol{\xi}^{\mathcal{B}}$ with associated bias $\boldsymbol{b_\xi}$ expressed in the body frame $\mathcal{B}$.

Differentiation of (2) gives

$$\dot{\lambda}_i = \frac{\partial \lambda_i}{\partial v_i^x}\frac{\mathrm{d}v_i^x}{\mathrm{d}t} + \frac{\partial \lambda_i}{\partial \omega_i}\frac{\mathrm{d}\omega_i}{\mathrm{d}t} = \frac{R_i\omega_i}{(v_i^x)^2}a_i^x - \frac{R_i}{v_i^x}\dot{\omega}_i. \tag{5}$$

Rearranging the slip definition (2) gives that

$$\frac{R_i\omega_i}{v_i^x} = 1 - \lambda_i, \tag{6}$$

and inserting (6) into the first term in (5), results in the following model of the slip dynamics:

$$\dot{\lambda}_i = \frac{1-\lambda_i}{v_i^x}a_i^x - \frac{R_i}{v_i^x}\dot{\omega}_i, \quad \forall i \in \{1, \dots, 4\}. \tag{7}$$

TABLE I

THE STATES USED IN THE DYNAMIC MODEL.

Notation	Description
$\boldsymbol{p} \in \mathbb{R}^2$	Position vector
$\boldsymbol{v} \in \mathbb{R}^2$	Velocity vector
$\boldsymbol{b_a} \in \mathbb{R}^2$	Accelerometer bias
$\boldsymbol{b_\xi} \in \mathbb{R}^2$	Gyroscope bias
$\phi \in \mathbb{R}$	Roll angle
$\psi \in \mathbb{R}$	Yaw angle
$\boldsymbol{\lambda} \in \mathbb{R}^4$	Wheel slip

To find a_i^x, it is convenient to utilize that the relation

$$\boldsymbol{a}_i = \boldsymbol{a}^{\mathcal{V}} + \ddot{\boldsymbol{\psi}} \times \boldsymbol{d}_i^{\mathcal{V}} + \dot{\boldsymbol{\psi}} \times (\dot{\boldsymbol{\psi}} \times \boldsymbol{d}_i^{\mathcal{V}}), \tag{8}$$

holds, where $\boldsymbol{a}_i^{\mathcal{V}}$ is the acceleration of a point P_i with coordinates $\boldsymbol{d}_i^{\mathcal{V}}$, and $\boldsymbol{\psi}$ is the rotation vector. The first and third terms in (8) can be found using the accelerometer and gyroscope measurements and their associated bias states. The second term, however, is not easily available. One option is to differentiate the gyro signal to provide an estimate, but investigations on the available datasets indicate that this term is small for large parts of the maneuver. Hence, in the following we neglect this term, but possible future work is to quantify how much this approximation affects estimation performance. In (8), $\dot{\psi}$ is replaced with (4f) and the acceleration $a^{\mathcal{V},X}$ is replaced with (3a) together with a small-angle approximation—that is,

$$\begin{aligned} \dot{\psi} &= u_{\boldsymbol{\xi}}^Z - b_{\boldsymbol{\xi}}^Z + w_{\boldsymbol{\xi}}^Z, \\ a^{\mathcal{V},X} &= u_{\boldsymbol{a}}^X - b_{\boldsymbol{a}}^X + w_{\boldsymbol{a}}^X. \end{aligned}$$

To summarize, the process model consists of (4) and (7). Table I explains the different states and their description.

B. Discrete-Time Dynamic Model

The dynamic model needs to be discretized to fit into the estimation framework. With the sampling period T_s, discretization of (4) and (7) yields the discrete-time model

$$\begin{aligned} \boldsymbol{p}_{k+1} &= \boldsymbol{p}_k + T_s \boldsymbol{v}_k \\ &\quad + \frac{T_s^2}{2} \boldsymbol{R}_{\mathcal{B}}^{\mathcal{I}} (\boldsymbol{u}_{\boldsymbol{a},k} - \boldsymbol{b}_{\boldsymbol{a},k} - \boldsymbol{g}_k + \boldsymbol{w}_{\boldsymbol{a},k}), && \text{(9a)} \\ \boldsymbol{v}_{k+1} &= \boldsymbol{v}_k \\ &\quad + T_s \boldsymbol{R}_{\mathcal{B}}^{\mathcal{I}} (\boldsymbol{u}_{\boldsymbol{a},k} - \boldsymbol{b}_{\boldsymbol{a},k} - \boldsymbol{g}_k + \boldsymbol{w}_{\boldsymbol{a},k}), && \text{(9b)} \\ \boldsymbol{b}_{\boldsymbol{a},k+1} &= \boldsymbol{b}_{\boldsymbol{a},k} + T_s \boldsymbol{w}_{\boldsymbol{b}_{\boldsymbol{a}},k}, && \text{(9c)} \\ \boldsymbol{b}_{\boldsymbol{\xi},k+1} &= \boldsymbol{b}_{\boldsymbol{\xi},k} + T_s \boldsymbol{w}_{\boldsymbol{b}_{\boldsymbol{\xi}},k}, && \text{(9d)} \\ \phi_{k+1} &= \phi_k + T_s (u_{\boldsymbol{\xi},k}^X - b_{\boldsymbol{\xi},k}^X + w_{\boldsymbol{\xi},k}^X), && \text{(9e)} \\ \psi_{k+1} &= \psi_k + T_s (u_{\boldsymbol{\xi},k}^Z - b_{\boldsymbol{\xi},k}^Z + w_{\boldsymbol{\xi},k}^Z), && \text{(9f)} \\ \lambda_{i,k+1} &= \lambda_{i,k} + T_s \left(\frac{1 - \lambda_{i,k}}{v_{i,k}^x} a_{i,k}^x - \frac{R_i}{v_{i,k}^x} (\dot{\omega}_{i,k} + w_{\dot{\omega},i}) \right). && \text{(9g)} \end{aligned}$$

In (9) we have used an Euler discretization, with second-order corrections for the acceleration components in (9a). In (9g) zero mean, white Gaussian noise terms $w_{\dot{\omega},i}$ for the wheel angular accelerations have been added. In total the input state vector is

$$\boldsymbol{u}_k = \begin{bmatrix} \boldsymbol{u}_{\boldsymbol{a},k}^{\mathrm{T}} & \boldsymbol{u}_{\boldsymbol{\xi},k}^{\mathrm{T}} & \dot{\boldsymbol{\omega}}_k^{\mathrm{T}} \end{bmatrix}^{\mathrm{T}} \in \mathbb{R}^8$$

The wheel angular accelerations, which are used as inputs, are not measured. These are estimated by a central-difference approximation using the wheel angular velocities measured by the ABS wheel-speed sensors.

C. Measurement Model

The first two elements in the measurement vector consist of the longitudinal and lateral GPS position measurements. To incorporate velocity information it is common to model the vehicle velocities in the body frame as measurements, either by using the wheel angular velocity measurements $\boldsymbol{\omega}_{m,k}$ together with the forward kinematics [14], [15], or employment of GPS velocity measurements [3], [16]. Both these approaches are valid in many scenarios. However, to estimate the slip when it is incorporated in the state equations, the wheel angular velocity measurements of each wheel are here used independently as elements of the measurement vector. The rationale for this is that it reduces observability issues.

The relation between the GPS position measurements $\boldsymbol{p}_{m,k}$ and the position $\boldsymbol{p}_k$ is

$$\boldsymbol{p}_{m,k} = \boldsymbol{p}_k + \boldsymbol{e}_{\boldsymbol{p},k},$$

where $\boldsymbol{e}_{\boldsymbol{p},k}$ is the GPS position measurement noise. To incorporate the wheel angular velocities, usage of the slip definition (2) gives

$$\lambda_i = 1 - \frac{R_i \omega_i}{v_i^x} \Leftrightarrow v_i^x \lambda_i = v_i^x - R_i \omega_i \Leftrightarrow R_i \omega_i = v_i^x (1 - \lambda_i)$$

Thus, the wheel angular velocity measurements $\boldsymbol{\omega}_{m,k}$ are at each time instant related to the states as

$$R_i \omega_{m,i} = v_i^x (1 - \lambda_i) + e_{\omega,i}, \quad i = 1, \ldots, 4, \tag{10}$$

where $\{e_{\omega,i}\}_{i=1}^4$ are the measurement-noise sources for the wheel-speed measurements. Eq. (10) measures a combination of λ_i, $\boldsymbol{v}$, ψ, ϕ, and the bias terms. However, because the contribution from the roll angle ϕ is small, it is hard to estimate ϕ from (10) alone. To improve roll-angle estimation, note that the acceleration of CoG is composed of a translational part and a rotational part—that is, it is possible to rewrite the Y-component of (3a) as

$$u_{\boldsymbol{a}}^Y \approx \dot{\psi} v^{\mathcal{V},X} + b_{\boldsymbol{a}}^Y + g\phi + w_{\boldsymbol{a}}^Y \tag{11}$$

where we, besides $\sin(\phi) \approx \phi$ and $\cos(\phi) \approx 1$, have assumed that the acceleration owing to $\dot{v}^{\mathcal{V},Y}$ is small. Insertion of (4f) into (11) yields

$$u_{\boldsymbol{a}}^Y \approx \left(u_{\boldsymbol{\xi}}^Z - b_{\boldsymbol{\xi}}^Z + w_{\boldsymbol{\xi}}^Z \right) v^{\mathcal{V},X} + b_{\boldsymbol{a}}^Y + g\phi + w_{\boldsymbol{a}}^Y. \tag{12}$$

Splitting up (12) into the standard measurement equation form results in the measurement equation

$$u_{\boldsymbol{a}}^Y = \left(u_{\boldsymbol{\xi}}^Z - b_{\boldsymbol{\xi}}^Z \right) v^{\mathcal{V},X} + b_{\boldsymbol{a}}^Y + g\phi + \begin{bmatrix} v^{\mathcal{V},X} & 1 \end{bmatrix} \begin{bmatrix} w_{\boldsymbol{\xi}}^Z & w_{\boldsymbol{a}}^Y \end{bmatrix}^{\mathrm{T}}.$$

To summarize, the measurement vector is

$$\boldsymbol{y}_k = \begin{bmatrix} \boldsymbol{p}_{m,k} & R_1 \omega_{m,1,k} & \cdots & R_4 \omega_{m,4,k} & u_{\boldsymbol{a},k}^Y \end{bmatrix}^{\mathrm{T}} \in \mathbb{R}^7.$$

V. Estimation Algorithm

To get the system on the same form as (1), it is necessary to partition the states into a linear part and a nonlinear part. It is computationally efficient to have as many states as possible in the linear part, since these are estimated with a Kalman filter. Consequently, only those states that contribute the most to the nonlinearities are in the nonlinear part.

A. Partitioning the States

The major nonlinearities are the velocities at the wheels, $v^x_{i,k}$, found in (9g). Since the wheel velocities depend on the yaw angle, longitudinal and translational vehicle velocites, the roll angle, and the bias terms, all these states can be modeled as nonlinear. However, with computational efficiency in mind, we only model the vehicle velocities and yaw angle as nonlinear, since these will dominate the contributions to $v^x_{i,k}$. The roll angle is assumed small, and is thus considered to be a linear state. Note that the yaw-rate measurement enters in $v^x_{i,k}$—that is, in the denominator in (9g)—which is not allowed in (1). Hence this term has to be linearized in the measurement update step. The slip is multiplied with the wheel acceleration in (9g), where the wheel acceleration depends on the bias terms and the process inputs. Introducing the four slip quantities as nonlinear states would drastically increase computational complexity. Thus $\{\lambda_{i,k}\}_{i=1}^4$ are considered to be linear.

In total there are three nonlinear states in $\boldsymbol{\eta}_k$ and 11 linear states in $\boldsymbol{z}_k$, which form the total state vector $\boldsymbol{x}_k = \begin{bmatrix}\boldsymbol{z}_k^{\mathrm{T}} & \boldsymbol{\eta}_k^{\mathrm{T}}\end{bmatrix}^{\mathrm{T}} \in \mathbb{R}^{14}$, where

$$\boldsymbol{\eta}_k = \begin{bmatrix}\boldsymbol{v}_k^{\mathrm{T}} & \psi_k\end{bmatrix}^{\mathrm{T}}, \quad \boldsymbol{z}_k = \begin{bmatrix}\boldsymbol{p}_k^{\mathrm{T}} & \boldsymbol{b}_{\boldsymbol{a},k}^{\mathrm{T}} & \boldsymbol{b}_{\boldsymbol{\xi},k}^{\mathrm{T}} & \phi_k & \boldsymbol{\lambda}_k^{\mathrm{T}}\end{bmatrix}. \tag{13}$$

B. Time Update

In the prediction steps of the RBPF the dynamics (9) are used to propagate the estimates $\hat{\boldsymbol{x}}_k^i$ to time index $k+1$. To propagate the covariances in the Kalman filter, however, linearization of the states in $\boldsymbol{z}_k^i$ that actually are nonlinear is required. With the partitioning (13), the matrices needed for (1a) and (1b) in the respective time-update step become

$$\begin{aligned}\boldsymbol{A}_k &= \left.\frac{\partial \boldsymbol{z}_{k+1}}{\partial \boldsymbol{z}_k}\right|_{\hat{\boldsymbol{x}}_k^i, \boldsymbol{u}_k}, \quad \boldsymbol{F}_k = \left.\frac{\partial \boldsymbol{z}_{k+1}}{\partial \boldsymbol{u}_k}\right|_{\hat{\boldsymbol{x}}_k^i, \boldsymbol{u}_k},\\ \boldsymbol{B}_k &= \left.\frac{\partial \boldsymbol{\eta}_{k+1}}{\partial \boldsymbol{z}_k}\right|_{\hat{\boldsymbol{x}}_k^i, \boldsymbol{u}_k}, \quad \boldsymbol{G}_k = \left.\frac{\partial \boldsymbol{\eta}_{k+1}}{\partial \boldsymbol{u}_k}\right|_{\hat{\boldsymbol{x}}_k^i, \boldsymbol{u}_k}.\end{aligned} \tag{14}$$

The inputs corresponding to $\boldsymbol{u}_k^{\boldsymbol{z}}$, $\boldsymbol{w}_k^{\boldsymbol{z}}$ and $\boldsymbol{u}_k^{\boldsymbol{\eta}}$, $\boldsymbol{w}_k^{\boldsymbol{\eta}}$ in (1) are

$$\begin{aligned}(\boldsymbol{u}_k^{\boldsymbol{z}})^{\mathrm{T}} &= \begin{bmatrix}\boldsymbol{u}_{\boldsymbol{a},k}^{\mathrm{T}} & \boldsymbol{b}_{\boldsymbol{a},k}^{\mathrm{T}} & \boldsymbol{u}_{\boldsymbol{\xi},k}^{\mathrm{T}} & \boldsymbol{b}_{\boldsymbol{\xi},k}^{\mathrm{T}} & \dot{\boldsymbol{\omega}}_k^{\mathrm{T}}\end{bmatrix}^{\mathrm{T}},\\ (\boldsymbol{w}_k^{\boldsymbol{z}})^{\mathrm{T}} &= \begin{bmatrix}\boldsymbol{w}_{\boldsymbol{a},k} & \boldsymbol{w}_{\boldsymbol{b}_{\boldsymbol{a}},k}^{\mathrm{T}} & \boldsymbol{w}_{\boldsymbol{\xi},k}^{\mathrm{T}} & \boldsymbol{w}_{\boldsymbol{b}_{\boldsymbol{\xi}},k}^{\mathrm{T}} & \boldsymbol{w}_{\dot{\boldsymbol{\omega}},k}^{\mathrm{T}}\end{bmatrix}^{\mathrm{T}},\\ (\boldsymbol{u}_k^{\boldsymbol{\eta}})^{\mathrm{T}} &= \begin{bmatrix}\boldsymbol{u}_{\boldsymbol{a},k}^{\mathrm{T}} & \boldsymbol{u}_{\boldsymbol{\xi},k}^{\mathrm{T}}\end{bmatrix}^{\mathrm{T}},\\ (\boldsymbol{w}_k^{\boldsymbol{\eta}})^{\mathrm{T}} &= \begin{bmatrix}\boldsymbol{w}_{\boldsymbol{a},k}^{\mathrm{T}} & \boldsymbol{w}_{\boldsymbol{\xi},k}^{\mathrm{T}}\end{bmatrix}^{\mathrm{T}}.\end{aligned} \tag{15}$$

The prediction consists of propagating the dynamics (9) based on the estimates at the previous time step and the covariance matrix for the linear states using (14) and (15).

C. Measurement Update

Similar to the prediction step, the measurement update step needs $\boldsymbol{C}_k$ in (1c), where some of the states have to be linearized to fit in the framework. The measurement matrices are computed as the first-order approximation

$$\boldsymbol{C}_k = \left.\frac{\partial \boldsymbol{y}_k}{\partial \boldsymbol{z}_k}\right|_{\hat{\boldsymbol{x}}_k^i, \boldsymbol{u}_k}. \tag{16}$$

VI. Experimental Results

The experimental results are from a test drive that was performed at a race track in Linköping, Sweden. To give an initial comparison, we have also implemented the approach to slip estimation in [17]. It is a rule-based velocity estimator that uses filtered versions of the angular velocities of the wheels and the longitudinal acceleration for estimating the velocity. It uses different sensor signals depending on if the vehicle is braking, accelerating, driving with approximately constant velocity, or if the velocity is very low.

A. Experimental Setup

The vehicle is a Volkswagen Golf V 2008, equipped with state-of-the-art sensors, see Fig. 3 and [18]. The sensors used in the estimation algorithms are:

- The wheel-angular velocities from the ABS wheel-speed sensors, sending measurements at 10 Hz.
- A GPS sensor, delivering position measurements at 4 Hz with an accuracy of approximately 2.5 m.
- An Xsens IMU [19] that executes at 100 Hz. Only the planar accelerations and the yaw and roll rates are used in the estimation algorithm. The IMU is approximately located at the (unloaded) mass center, nearly aligned with the vehicle's coordinate system, during the experiments. No actions are taken to account for the location error or misalignment.

In addition, the vehicle is equipped with high-precision roll- and pitch-angle sensors (accuracy 0.07 deg at 250 Hz), as well as an optical sensor for measuring the longitudinal velocity with high precision (0.1% at 250 Hz). By using the wheel-speed measurements together with measurements of the longitudinal velocity, it is possible to extract information about longitudinal wheel slip with high accuracy.

Remark 1: The effective tire radius R_i was determined by logging data during steady-state, straight-line driving and comparing the measured longitudinal velocity v^X with the wheel angular velocity ω_i. The effective wheel radius for each wheel was then chosen as $R_i = v^X/\omega_i$.

B. Results

This scenario was constructed by driving approximately seven laps on a small part of a race track. Fig. 4 shows the GPS positions for approximately one lap of the scenario together with the position estimates. The measured and longitudinal velocity are shown in Fig. 5 for the whole test drive. A major part of the available friction is used during cornering and the braking behavior is aggressive.

Fig. 3. The vehicle testbed used in the experiments. The velocity sensor is placed at the front end, aligned with the longitudinal axis. The roll and pitch angle sensors are situated at the front end and in front of the rear wheels. The vehicle was also equipped with a GPS receiver during the experiments.

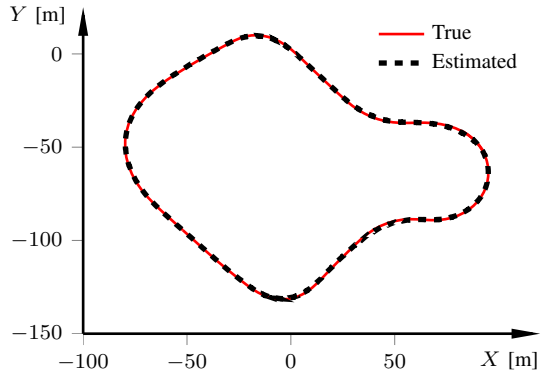

Fig. 4. The estimated positions and GPS positions for one lap on the considered race track.

Fig. 6 shows a 25 s excerpt of the maneuver. The maximum velocity error in this figure is approximately 0.6 m/s. The roll-angle estimation is consistent in most parts, and the slip estimates are highly accurate. Fig. 7 displays the wheel slip for the second and fourth wheel, respectively, together with the rule-based slip estimation algorithm in [17][1] for another 25 s excerpt. We have confirmed that the approach in [17] performs well when driving approximately straight. For this dataset, however, the slip estimation with the method proposed in this paper is superior, and also rapid changes in the slip are handled well. The slip characteristics between the second and fourth wheels are different. This is because the vehicle is front-wheel driven in combination with significant load transfer in both roll and pitch direction, owing to large acceleration/deceleration as well as aggressive cornering. Fig. 8 provides the likelihood of the time-averaged root-mean-square errors as cumulative functions over the 100 executions for different number of particles. The average error for λ_1 is 0.025 (and is similar for the other wheels), and approximately 95% of the executions yield an average velocity error of less than 1 m/s when using 400 particles.

The average computation time in MATLAB for one iteration of the algorithm when using 400 particles is approximately 5 ms. The algorithm scales linearly in the number of particles [21], and for 1000 particles the average computation time is approximately 12 ms in the current implementation. Hence, with a dedicated implementation the algorithm can execute in real time.

[1]The parameters used in that algorithm are chosen as suggested in [17].

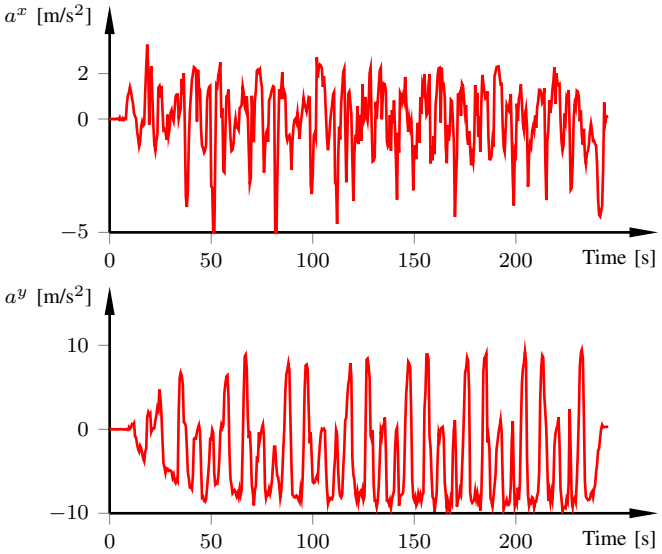

Fig. 5. The accelerations as measured by the accelerometer in the experimental evaluation. The driving behavior is aggressive, and utilizes the available friction in both longitudinal and lateral direction. The maneuver is performed on dry asphalt, where the friction coefficient μ typically is in the range $0.95 \leq \mu \leq 1.2$ [2], [20].

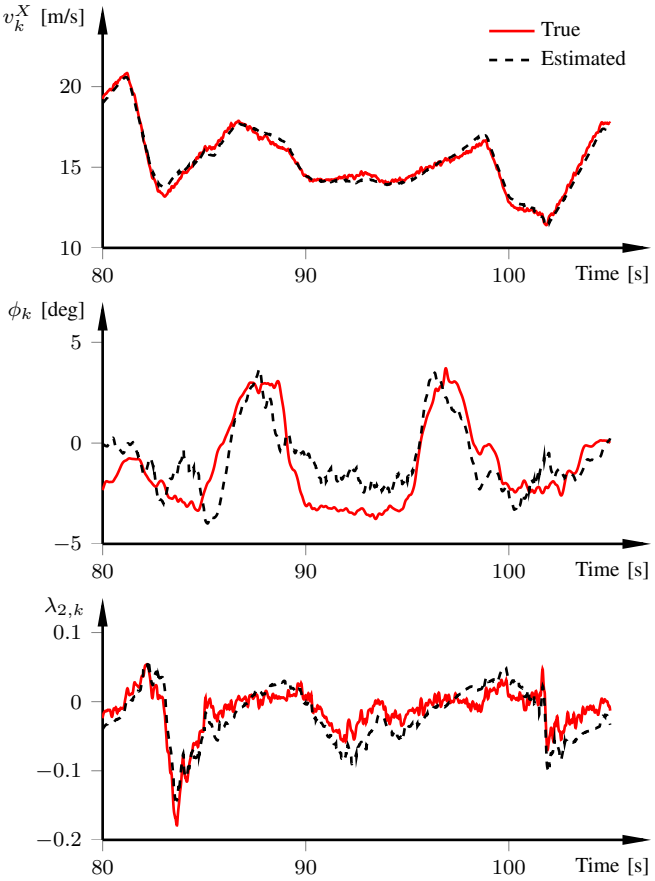

Fig. 6. Estimated (black dashed) and ground truth (red) velocity, roll angle, and wheel slip for a portion of the whole dataset. The peak in the force curve occurs when $\lambda \approx \pm 0.15$ (see Fig. 1 and [20]). The results are representative of what can be expected from a typical filter realization.

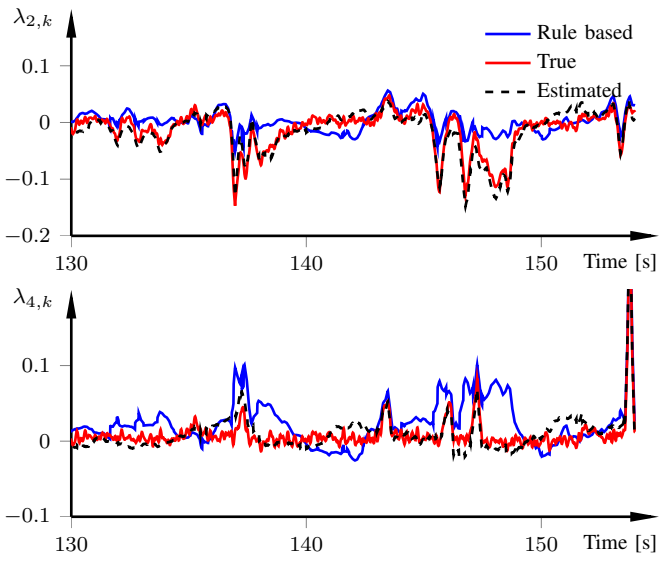

Fig. 7. Estimated (dashed) and ground truth (red) wheel slip for a portion of the whole dataset. For comparison, the slip estimation approach in [17] is also shown (blue). The considered dataset contains combined longitudinal and lateral movement, in addition to significant roll. This puts large demands on modeling coupling effects, something which the proposed method does.

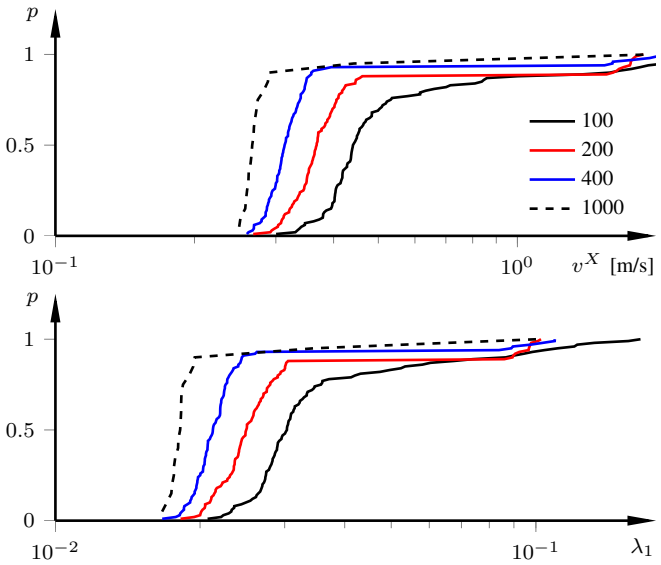

Fig. 8. The probability of time-averaged root-mean-square error for different number of particles, computed as cumulative distribution functions over 100 executions of the whole dataset. Out of the 100 executions, 99 give a velocity error smaller than 0.7 m/s when using 1000 particles. Moreover, over 90 give a velocity error of less than 0.27 m/s and slip error of less than 0.02. The estimation performance for 400 particles is also good, whereas using less than 400 particles clearly degrades performance.

VII. Conclusions

The presented method uses a single estimator for estimating states tightly connected to vehicle safety systems. In this way, the slip dynamics can explicitly be accounted for in the estimation algorithm. It is the author's belief that modeling these states simultaneously can improve estimation accuracy, because more effects are taken into account. It is future work to quantify the performance difference to current state-of-the-art methods. However, the results show that the estimation performance is highly promising.

Acknowledgment

The author thanks K. Lundahl at the Vehicular Systems Division, Linköping University, Sweden, for the datasets.

References

[1] T. B. Schön, F. Gustafsson, and P.-J. Nordlund, "Marginalized particle filters for mixed linear nonlinear state-space models," *IEEE Trans. Signal Process.*, vol. 53, no. 7, pp. 2279–2289, 2005.

[2] J. Svendenius, "Tire modeling and friction estimation," Ph.D. dissertation, Department of Automatic Control, Lund University, Sweden, Apr. 2007.

[3] C. C. Ward and K. Iagnemma, "A dynamic-model-based wheel slip detector for mobile robots on outdoor terrain," *IEEE Trans. Robot.*, vol. 24, no. 4, pp. 821–831, 2008.

[4] F. Gustafsson, "Slip-based tire-road friction estimation," *Automatica*, vol. 33, no. 6, pp. 1087–1099, 1997.

[5] C. R. Carlson and J. C. Gerdes, "Consistent nonlinear estimation of longitudinal tire stiffness and effective radius," *IEEE Trans. Control Syst. Technol.*, vol. 13, no. 6, pp. 1010–1020, 2005.

[6] S. Miller, B. Youngberg, A. Millie, S. Patrich, and J. C. Gerdes, "Calculating longitudinal wheel slip and tire parameters using GPS velocity," in *Am. Control Conf.*, Arlington, VA, Jun. 2001.

[7] L. Ojeda, D. Cruz, G. Reina, and J. Borenstein, "Current-based slippage detection and odometry correction for mobile robots and planetary rovers," *IEEE Trans. Robot.*, vol. 22, no. 2, pp. 366–378, 2006.

[8] L. R. Ray, "Nonlinear tire force estimation and road friction identification: Simulation and experiments,," *Automatica*, vol. 33, no. 10, pp. 1819–1833, 1997.

[9] M. Lghani, "Road bank and vehicle roll angles estimation based on proportional-integral observer," in *8th IFAC Symp. Fault Detect., Superv. Safety Tech. Processes*, Mexico City, Mexico, Aug. 2012.

[10] H. Grip, L. Imsland, T. Johansen, J. Kalkkuhl, and A. Suissa, "Estimation of road inclination and bank angle in automotive vehicles," in *Am. Control Conf.*, St. Louis, MI, Jun. 2009.

[11] J. Ryu and J. C. Gerdes, "Estimation of vehicle roll and road bank angle," in *Am. Control Conf.*, Boston, MA, Jun. 2004.

[12] M. Arulampalam, S. Maskell, N. Gordon, and T. Clapp, "A tutorial on particle filters for online nonlinear/non-Gaussian Bayesian tracking," *IEEE Trans. Signal Process.*, vol. 50, no. 2, pp. 174–188, 2002.

[13] K. Berntorp, "Particle filtering and optimal control for vehicles and robots," Ph.D. dissertation, Department of Automatic Control, Lund University, Sweden, May 2014.

[14] J. Yi, H. Wang, J. Zhang, D. Song, S. Jayasuriya, and J. Liu, "Kinematic modeling and analysis of skid-steered mobile robots with applications to low-cost inertial-measurement-unit-based motion estimation," *IEEE Trans. Robot.*, vol. 25, no. 5, pp. 1087–1097, 2009.

[15] K. Berntorp, K.-E. Årzén, and A. Robertsson, "Sensor fusion for motion estimation of mobile robots with compensation for out-of-sequence measurements," in *11th Int. Conf. Control, Automation and Systems*, Gyeonggi-do, Korea, Oct. 2011.

[16] K. Iagnemma and C. C. Ward, "Classification-based wheel slip detection and detector fusion for mobile robots on outdoor terrain," *Auton. Robots*, vol. 26, no. 1, pp. 33–46, 2009.

[17] S. M. Savaresi and M. Tanelli, *Active Braking Control Systems Design for Vehicles*. Wiesbaden, Germany: Springer-Verlag Gmbh, 2010.

[18] K. Lundahl, J. Åslund, and L. Nielsen, "Vehicle dynamics platform, experiments, and modeling aiming at critical maneuver handling," Department of Electrical Engineering, Linköping University, SE-581 83 Linköping, Sweden, Tech. Rep. LiTH-R-3064, Jun. 2013.

[19] N. Xsens Technologies B.V., "MTi and MTx User Manual and Technical Documentation," 2010, http://www.xsens.com.

[20] B. Olofsson, K. Lundahl, K. Berntorp, and L. Nielsen, "An investigation of optimal vehicle maneuvers for different road conditions," in *7th IFAC Symp. Adv. Automotive Control*, Tokyo, Japan, Sep. 2013.

[21] R. Karlsson, T. Schön, and F. Gustafsson, "Complexity analysis of the marginalized particle filter," *IEEE Trans. Acoust., Speech, Signal Process.*, vol. 53, no. 11, pp. 4408–4411, 2005.